Linear Stability of Taylor-Couette Flows with Axial Heat Buoyancy *

CHEN Jian-Guo(陈建国)[1,2**], REN Ling(任玲)[3], FU Song(符松)[3]

[1]*Center for Public Safety Research, Tsinghua University, Beijing 100084*
[2]*Department of Engineering Physics, Tsinghua University, Beijing 100084*
[3]*Department of Engineering Mechanics, Tsinghua University, Beijing 100084*

(Received 25 April 2006)

The linear stability is studied of flows confined between two concentric cylinders, in which the radial temperature gradient and axial gravity are considered for an incompressible Newtonian fluid. Numerical method based on the Petrov–Galerkin scheme is developed to deal with the buoyancy term in momentum equations and an additional temperature perturbation equation. Computations of the neutral stability curves are performed for different rotation cases. It is found that the flow instability is influenced by both centrifugal and axial shear instabilities, and the two instability mechanisms interact with each other. The outer cylinder rotation plays dual roles of stabilizer and destabilizer under different rotating stages with the inner cylinder at rest. For the heat buoyancy-induced axial flow, spiral structures are found in the instability modes.

PACS: 47. 15. Fe, 47. 20. Gv

It is well known that some processes, which are frequently encountered in industry, such as the cooling of rotating electric machinery,[1] or purification of industrial waste water,[2] can be considered as flows confined between two concentric rotating cylinders, the so-called Taylor–Couette flow. A typical flow is a non-zero shear flow in axial direction combined with a rotation of one or two cylinders. The comparatively complex properties and stability of the flow will affect the efficiency of fluids mixture and transportation. It is therefore of great significance to investigate the possible instability in such flows.

The instability of rotating flow combined with an axial flow, reflecting the competition between different physical mechanisms of instability, has caught great interests of many researchers. Examples include the Hagen–Poiseuille flow under the conditions of rotation and axial pressure gradient;[3] the spiral Couette flow of rotation and axial sliding;[4] the spiral Poiseuille flow of rotation and axial pressure gradient.[5] All the above investigations do not consider the existence of temperature and gravity. However, in the realistic industry, buoyancy-induced heat convection plays an important role in Taylor–Couette problems. Therefore, the linear stability is investigated here of flows confined between two concentric cylinders rotating independently and with axial heat buoyancy caused by the axial gravity and radial temperature gradient, as shown in Fig. 1.

The Petrov–Galerkin method is an ideally available and efficient tool for studying the linear instability of composite rotating and axial flows, such as the spiral Couette flow with axial sliding[4] and the spiral Poiseuille flow with axial pressure gradient between two concentric rotating cylinders.[5] The method is also valid for analysing the linear stability of the present problem, where the rotating flow between two concentric cylinders combines with the axial shear flow induced by the radial temperature gradient and gravity. However, the Petrov–Galerkin method has to be developed because of the occurrence of buoyancy term in momentum equations and an additional temperature perturbation equation, discussed in detail as follows.

We consider an incompressible Newtonian fluid of kinematics viscosity ν and density ρ contained between two concentric rotating infinite cylinders whose radii, angular velocities and temperatures of inner and outer cylinders are r_i^*, r_o^*, Ω_i, Ω_o and $T_d/2$, $-T_d/2$, respectively. Introducing the gap between the cylinders $d = r_o^* - r_i^*$, the radius ratio $\varepsilon = r_i^*/r_o^*$ and temperature difference T_d, all variables will be rendered dimensionless using d, d^2/ν, ν^2/d^2, T_d. The dimensionless continuity, momentum (Navier–Stokes) and energy equations can be written as

$$\nabla \cdot \boldsymbol{v} = 0, \tag{1a}$$

$$\partial_t \boldsymbol{v} + (\boldsymbol{v} \cdot \nabla)\boldsymbol{v} = -\nabla P + \Delta \boldsymbol{v} + GrT\boldsymbol{e}_z, \tag{1b}$$

$$\partial_t T + (\boldsymbol{v} \cdot \nabla)T = \frac{1}{Pr}\Delta T, \tag{1c}$$

where $Gr = \rho g d^2 T_d/\nu^2$ is the Grashof number, and Pr is the Prandtl number. Here the Boussinesq approximation is invoked for the buoyancy term, and constant fluid properties are assumed.

Let (u, v, w) be the physical components of the velocity $\boldsymbol{v}$ in cylindrical coordinates (r, θ, z). Dimensionless non-slip velocity and constant temperature boundary conditions at the inner and outer cylinders are $u(r_i) = u(r_o) = w(r_i) = w(r_o) = 0$, $v(r_i) = Re_i$, $v(r_o) = Re_o$, and $T(r_i) = 0.5$, $T(r_o) = 0.5$, where $r_i = \varepsilon/(1-\varepsilon)$ and $r_o = 1/(1-\varepsilon)$. The Couette flow Reynolds numbers are $Re_i = r_i^* d\Omega_i/\nu$ and $Re_o = r_o^* d\Omega_o/\nu$ for the rotating cylinders. The basic

* Supported by the National Key Basic Research and Development Programme of China under Grant No 2001CB409600.
** Email: chenjianguo@tsinghua.edu.cn
©2006 Chinese Physical Society and IOP Publishing Ltd

solution $\boldsymbol{v}_B$ and T_B are

$$u_B = 0,\ v_B = Ar + B/r,\ T_B = C_1 \ln r + C_2,$$
$$w_B = C_3 r^2 \ln r + C_4 r^2 + C_5 \ln r + C_6, \tag{2}$$

where the constants A, B and C_i are given by

$$A = \frac{Re_0 - \varepsilon Re_i}{1+\varepsilon}, \quad B = \frac{\varepsilon(Re_i - \varepsilon Re_0)}{(1-\varepsilon)(1-\varepsilon^2)},$$
$$C_1 = \frac{1}{\ln \varepsilon}, \quad C_2 = -\frac{1}{2} + \frac{\ln(1-\varepsilon)}{\ln \varepsilon},$$
$$C_3 = -\frac{Gr}{4} C_1, \quad C_4 = \frac{Gr}{4}(C_1 - C_2),$$
$$C_5 = \frac{[C_3(r_o^2 \ln r_o - r_i^2 \ln r_i) + C_4(r_o^2 - r_i^2)]}{(\ln r_i - \ln r_o)},$$
$$C_6 = -C_3 r_i^2 \ln r_i - C_4 r_i^2 - C_5 \ln r_i. \tag{3}$$

Suppose the basic solution is perturbed slightly, the linearized differential equations satisfied by the disturbance are found to be

$$\nabla \cdot \boldsymbol{u}' = 0, \tag{4a}$$
$$\partial_t \boldsymbol{u}' + (\boldsymbol{v}_B \cdot \nabla)\boldsymbol{u}' + (\boldsymbol{u}' \cdot \nabla)\boldsymbol{v}_B = -\nabla p' + \Delta \boldsymbol{u}' + GrT'\boldsymbol{e}_z, \tag{4b}$$
$$\partial_t T' + (\boldsymbol{v}_B \cdot \nabla)T' + \nabla T_B \cdot \boldsymbol{u}' = \frac{1}{Pr}\Delta T'. \tag{4c}$$

The disturbance is assumed to vary periodically in the azimuthal and axial directions,

$$\boldsymbol{u}'(r,\theta,z,t) = \boldsymbol{u}(r) e^{i(n\theta + kz) + \lambda t}, \tag{5a}$$
$$p'(r,\theta,z,t) = p(r) e^{i(n\theta + kz) + \lambda t}, \tag{5b}$$
$$T'(r,\theta,z,t) = T(r) e^{i(n\theta + kz) + \lambda t}. \tag{5c}$$

The disturbance amplitudes $\boldsymbol{u}$ and T satisfy the homogeneous boundary conditions, i.e., $\boldsymbol{u}(r_i) = \boldsymbol{u}(r_o) = 0$ and $T(r_i) = T(r_o) = 0$.

The spatial discretization for numerically solving Eq. (4) is obtained by projecting Eq. (4) onto a suitable basis. The space of divergence-free vector fields satisfying the boundary conditions is

$$V = \{\boldsymbol{u} \in (\Pi(r_i, r_o))^3 | \nabla \cdot \boldsymbol{u} = 0,\ \boldsymbol{u}(r_i) = \boldsymbol{u}(r_o) = 0\}, \tag{6}$$

where $(\Pi(r_i, r_o))^3$ is the Hilbert space of square-integrable vectorial-functions defined in the interval (r_i, r_o), with the inner product $\langle \boldsymbol{u}, \boldsymbol{v} \rangle = \int_{r_i}^{r_o} \bar{\boldsymbol{u}} \cdot \boldsymbol{v} r dr$, where $\bar{\boldsymbol{u}}$ denotes the complex conjugate of $\boldsymbol{u}$. For any $\boldsymbol{u} \in V$ and any function P, we have $\langle \boldsymbol{u}, \nabla P \rangle = 0$ according to the Gauss integral. Expanding $\boldsymbol{u}$ in a suitable basis of V, we can acquire

$$\boldsymbol{u} = \sum_\alpha a_\alpha \boldsymbol{u}_\alpha, \quad \boldsymbol{u}_\alpha \in V. \tag{7}$$

Substituting Eqs. (5) and (7) into Eq. (4), the continuity equation (4a) is satisfied identically. Projecting the linearized Eq. (4b) onto V, the pressure term disappears and a linear system for the coefficients a_α is obtained by

$$\lambda \sum_\beta \langle \tilde{\boldsymbol{u}}_\alpha, \boldsymbol{u}_\beta \rangle a_\beta = \sum_\beta \langle \tilde{\boldsymbol{u}}_\alpha, \boldsymbol{v}_B \cdot \nabla \boldsymbol{u}_\beta + \boldsymbol{u}_\beta \cdot \nabla \boldsymbol{v}_B - \Delta \boldsymbol{u} + Gr T_\beta \rangle. \tag{8}$$

Implement a Petrov–Galerkin scheme,[6,7] where the basis used to expand the unknown velocity $\{\boldsymbol{u}_\alpha\}$ differs from that used to project the equations of $\{\tilde{\boldsymbol{u}}_\alpha\}$. The divergence-free condition for a velocity field of the form Eq. (5a) is $D_+ u + inv/r + ikw = 0$, and a basis for V is obtained by taking $\boldsymbol{u}_j^1 = (0, -rkh_j(r), nh_j(r))$, $\boldsymbol{u}_j^2 = (-ikf_j(r), 0, D_+ f_j(r))$, where $D = \partial_r$, $D_+ = D + 1/r$. The functions f_j and h_j at the two cylinders should satisfy the homogeneous boundary conditions.

Introducing a new radial coordinate $x = 2(r - r_i) - 1$, $x \in [-1, +1]$ and using Chebyshev polynomials T_j, f_j and h_j satisfying the homogeneous boundary conditions at the two cylinders can be simply chosen as $f_j(r) = (1-x^2)^2 T_j(x)$ and $h_j(r) = (1-x^2)T_j(x)$. Thus all the inner products in Eq. (8) can be numerically computed by Gauss–Lobatto quadrature.

Furthermore, the expansion of the temperature disturbance amplitude T is in a similar way to that of the velocity disturbance amplitude $\boldsymbol{u}$. Considering T satisfying the homogeneous boundary conditions at the two cylinders, we choose

$$T(r) = b_j h_j(r). \tag{9}$$

Finally we obtain a generalized complex eigenvalue system of the form

$$\boldsymbol{H}\boldsymbol{x} = \lambda \boldsymbol{G}\boldsymbol{x}, \tag{10}$$

where the vector $\boldsymbol{x}$ contains the real and imaginary parts of the coefficients a_α and b_j defined in Eqs. (7) and (9), H and $\boldsymbol{G}$ are $N \times N$ constant matrices, where N denotes the number of Chebyshev collocation points. Then the eigenvalue problem of Eq. (10) can be written in the functional form

$$\lambda = \lambda(Re_i, Re_o, Gr, Pr, k, n, \varepsilon). \tag{11}$$

For the flow media specified, Pr is fixed, such as it equals to 0.709 for the air. We restrict the computations to the $\varepsilon = 0.5$ case and the number of spectral modes considered for the computation is $N = 24$.

Define the real part of λ, $\mathrm{Re}\lambda$, to be the real part of the first eigenvalue of the linear system Eq. (11) which crosses the imaginary axis. For given Re_i, Re_o and n, the curves of $\mathrm{Re}\lambda = 0$ in (k, Gr)-plane are termed neutral stability curves (NSC). For fixed Re_i, Re_o, and given n, k, $\mathrm{Re}\lambda = 0$ corresponds to the Grashof number $Gr_c(n,k)$. The critical Grashof number is given by $Gr_{\mathrm{crit}} = \min_{n,k} Gr_c(n,k)$, and the corresponding values of n, k are the critical azimuthal and axial wavenumbers n_{crit} and k_{crit}.

Figure 2 gives the NSC in (k, Gr)-plane for various integer values of azimuthal wavenumber with $Re_i = 0$ and $Re_o = 0$. Under this condition, the basic flow with no-rotation is only induced by the axial heat buoyancy. It can be seen from Fig. 2 that the absolute minimum of the set of the NSC corresponds to $n_{\mathrm{crit}} = 1$, where the critical axial wavenumber and Grashof number are

$k_{\rm crit} = 2.63$ and $Gr_{\rm crit} = 11801.4$, respectively. The corresponding geometrical shape of the critical eigenfunction (instability mode) is a spiral flow, as is shown in Fig. 3(c). A key parameter to depict the spiral pattern is a spiral angle with a constant-z plane, which depends on the wavenumbers n, k and the imaginary part of the critical eigenvalue.[4] Figure 3(c) shows the contour surface of perturbed stream function with the spiral angle of 10.76°. The isolines of perturbed stream function and temperature are also illustrated in Figs. 3(a) and 3(b).

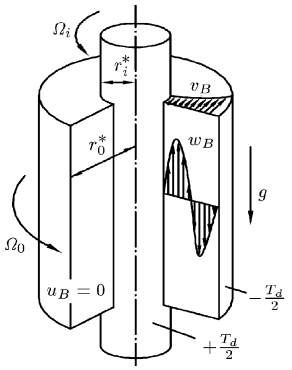

Fig. 1. Geometric sketch and parameters of Taylor–Couette flow with heat convection induced by radial temperature gradient and axial gravity.

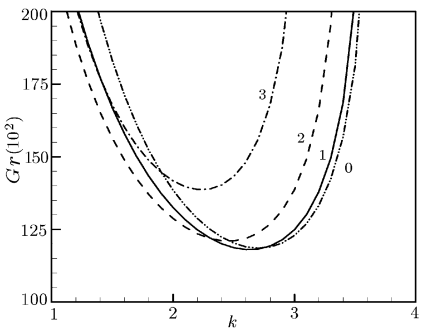

Fig. 2. Neutral stability curves with $Re_i = 0$ and $Re_o = 0$. The numbers on curves indicate the azimuthal wavenumbers.

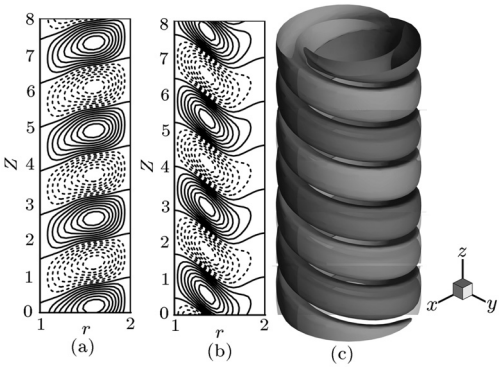

Fig. 3. Isolines of (a) perturbed stream function and (b) perturbed temperature in the (r, z)-plane. The dashed line denotes negative value. (c) Contour surface of perturbed stream function is a spiral pattern.

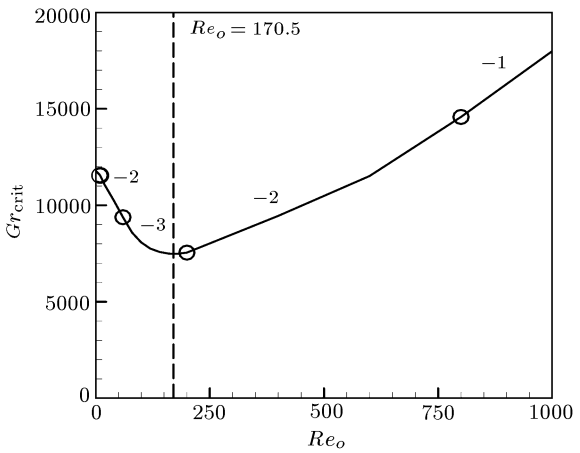

Fig. 4. Critical Grashof number versus Re_o when $Re_i = 0$. The number in each segment indicates the dominant azimuthal wavenumber. The circles represent the transitions between different $n_{\rm crit}$.

When $Re_i = 0$ and $Re_o \neq 0$ for a stationary inner cylinder, the NSC in (k, Gr)-plane is similar to the curves in Fig. 2 at different Re_o. In this case, the critical numbers $Gr_{\rm crit}$, $n_{\rm crit}$ and $k_{\rm crit}$ can be obtained for Re_o fixed. The critical $Gr_{\rm crit}$ is shown in Fig. 4 as a function of Re_o with $n_{\rm crit}$ labeled. When $Re_o = 0$, the physical system regresses to the above mentioned case (see Figs. 2 and 3) with the shear instability induced by the axial heat buoyancy. It can be seen from Fig. 4 that the shear instability is suggested to be the dominant instability mechanism with the increase of Re_o. Moreover, the outer rotation Reynolds number (rotating velocity of outer cylinder) plays dual roles to the flow instability. In the region of low rotating velocity with $Re_o < 170.5$, $Gr_{\rm crit}$ decreases when Re_o increases, the corresponding dominant azimuthal wavenumber changing by one unit. That shows the rotation of the outer cylinder has a destabilizing effect on the basic flow. However, in high rotating velocity region, $Gr_{\rm crit}$ increases with increasing Re_o, the corresponding critical azimuthal wavenumber changing by two units. It shows the effect of the rotation of the outer cylinder on the flow instability is stabilizing in this region.

For $Re_i \neq 0$ and $Re_o = 0$ with the outer cylinder at rest, the NSC in (k, Gr)-plane is displayed in Fig. 5 at different Re_i. For $Re_i = 20$, the dominant mode is $n_{\rm crit} = -2$, giving $Gr_{\rm crit} = 11083.2$ and $k_{\rm crit} = 2.50$; while for $Re_i = 30$, the neutral stability curve of the $n_{\rm crit} = -3$ mode develops a tail (sharp geometrical form) of instability for a much lower $Gr_{\rm crit} = 3479.7$, introducing a discontinuity in $Gr_{\rm crit}$. The position of all the extrema $Gr_{\rm crit}$ in NSC as a function of Re_i is plotted in Fig. 6, where a first-order discontinuity (discontinuity in the derivative) in $Gr_{\rm crit}$ can be observed with two solid curves across the point of $Re_i = 27.45$. The solid curve in Fig. 6 gives the absolute minimum, and the dashed curve corresponds to the other extremum. Before the crossing, such as in Fig. 5(a) for $Re_i = 20$, the NSC for $n_{\rm crit} = -3$ has a single extremum, while the minimum giving the critical parameter values $(k_{\rm crit}, Gr_{\rm crit})$ corresponds to $n_{\rm crit} = -2$. After crossing and due to the presence of the tail, the NSC has two extrema (minima) at the same $n_{\rm crit}$ mode, as shown in Fig. 5(b). $Gr_{\rm crit}$ exhibits multivalued branches as a function of Re_i as soon as the tail of instability appears. The tail of instability is very small at first, becoming larger until it merges with other

parts (see Fig. 5(c). with $Re_i = 49$). The occurrence of the mergence is depicted as $Gr_{\rm crit}$ changing with a vertical decrease at about $Re_i = 43$ (the crossing of solid and dashed curves) in Fig. 6. The appearance of tail can be explained as the competition between the shear instability mechanism induced by the axial heat buoyancy and the centrifugal instability mechanism characteristic of the Taylor-Couette problem. Figure 6 makes it evident that the shear instability plays a significant role prior to the onset of centrifugal instability when $Re_i = 0$. The centrifugal instability appears and comes into play as Re_i is increased. The shear instability seems to be the dominant mechanism except after the crossing of solid curves in Fig. 6, where a centrifugal instability becomes dominant. The crossing of solid curves can be thought of as the dominance transition between both the mechanisms. Moreover, the inner rotation Reynolds number approaches an asymptotic value which is $Re_i^{\infty} = 26.8$ in the centrifugal branch.

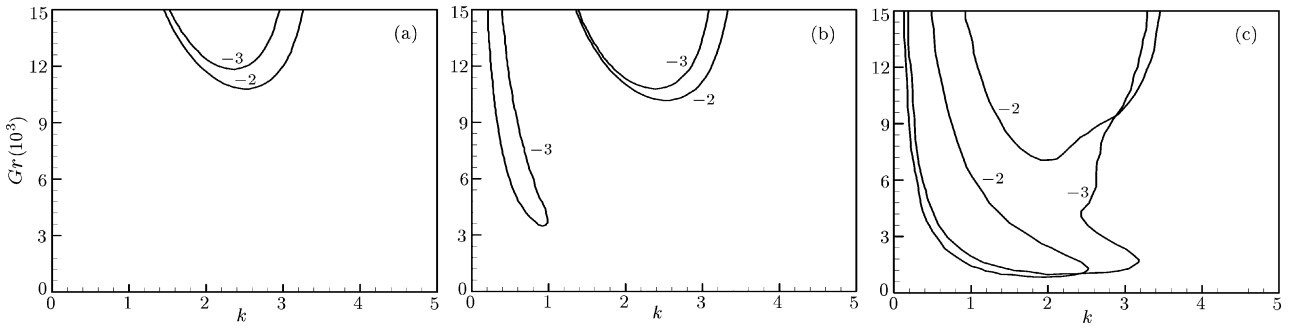

Fig. 5. Formation and evolution of a tail of instability for (a) $Re_i = 20$, (b) $Re_i = 30$ and (c) $Re_i = 49$ when $Re_o = 0$.

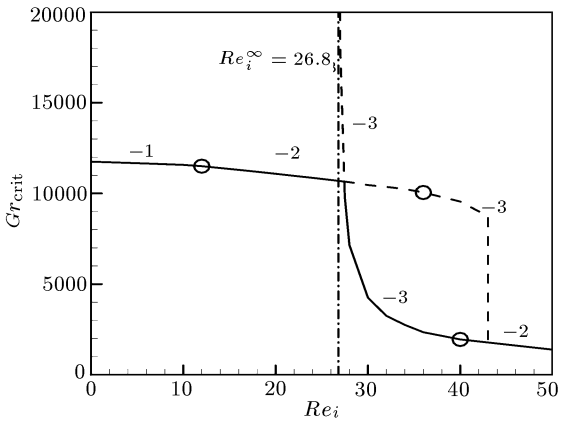

Fig. 6. Dependence of $Gr_{\rm crit}$ on Re_i for $Re_o = 0$.

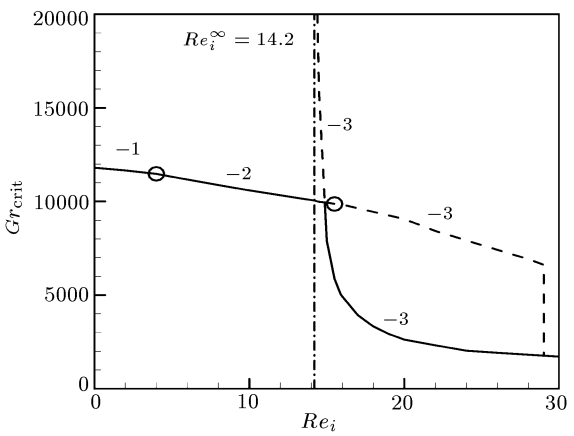

Fig. 7. Dependence of $Gr_{\rm crit}$ on Re_i for $Re_i/Re_o = 0.5$.

The similar behaviour is also found in the rigid rotation case $\Omega_i = \Omega_o$ (or equivalently $Re_i/Re_o = \varepsilon$, here $Re_i/Re_o = 0.5$). The dependence of $Gr_{\rm crit}$ on Re_i, reflecting the instability mechanisms competition, is given in Fig. 7, where a first-order discontinuity of $Re_i = 14.87$ and a mergence point at about $Re_i = 29$ are also found. As $Gr_{\rm crit}$ is increased, the centrifugal branch has an asymptotic value, being the asymptotic inner rotation Reynolds number $Re_i^{\infty} = 14.2$.

As can be seen from the above discussions, the NSC for this problem may have multiple extrema, and exhibit disconnected parts and sharp geometrical forms. All these features make the numerical computation of the critical parameters very difficult from the algorithmic point of view and time-consuming. More detailed analyses may be examined. For example, an extensive description of the linear instability of the physical system may be carried out by obtaining the critical surface $Gr_{\rm crit}$ (Re_i, Re_o) for a wide range of angular velocities of both cylinders. In addition, the present exploration is only concerned with the wide gap case $\varepsilon = 0.5$, while the linear stability with different radius ratios, such as the case close to the narrow gap ($\varepsilon \to 1$), may have new features and deserves further research.

References

[1] Becker K M and Kaye J 1962 *J. Heat Transf. Trans. ASME* **84** 97
[2] Ollis D F et al 1991 *Environ. Sci. Technol.* **25** 1523
[3] Cotton F W and Salwen H 1981 *J. Fluid Mech.* **108** 101
[4] Meseguer A and Marques F 2000 *J. Fluid Mech.* **402** 33
[5] Meseguer A and Marques F 2002 *J. Fluid Mech.* **455** 129
[6] Moser R D et al 1983 *J. Comput. Phys.* **52** 524
[7] Canuto C et al 1988 *Spectral Methods in Fluid Dynamics* (New York: Springer)